WAVE: A 3D Online Previewing Framework for Big Data Archives

Nicholas Tan Jerome, Suren Chilingaryan, Andrei Shkarin, Andreas Kopmann, Michael Zapf, Alexander Lizin and Till Bergmann
Institute for Data Processing and Electronics (IPE), Karlsruhe Institute of Technology (KIT), Eggenstein-Leopoldshafen, Germany

Keywords: Web-based Visualization, Scientific Visualization, Multi-resolution Slicemap, Visual Data Browsing.

Abstract: With data sets growing beyond terabytes or even petabytes in scientific experiments, there is a trend of keeping data at storage facilities and providing remote cloud-based services for analysis. However, accessing these data sets remotely is cumbersome due to additional network latency and incomplete metadata description. To ease data browsing on remote data archives, our WAVE framework applies an intelligent cache management to provide scientists with a visual feedback on the large data set interactively. In this paper, we present methods to reduce the data set size while preserving visual quality. Our framework supports volume rendering and surface rendering for data inspection and analysis. Furthermore, we enable a zoom-on-demand approach, where a selected volumetric region is reloaded with higher details. Finally, we evaluated the WAVE framework using a data set from the entomology science research.

1 INTRODUCTION

As part of scientific discovery process, the rate of data generation in science has increased dramatically (Szalay and Gray, 2006). Taking an entomology experiment from the ANKA synchrotron facility as an example (Ressmann et al., 2014), each sample scanned at the beamline station yields a data size ranging from 32 GB to 150 GB. There are thousands of data sets produced monthly resulting in terabytes and perhaps petabytes of data.

To handle such a large amount of data, a new trend in data management policy arises, where experiment data are kept at the facility while providing cloud-based services for external analysis. Initially, data are stored at the data processing server during experiment phase. But when these data are no longer in active use, they are moved to a long-term archive for better data retention, e.g. magnetic tapes or optical disks. However, accessing these archived data remotely introduces additional latency. If scientists wish to retrieve these data sets, they often refer to the associated metadata. There is no guarantee that the metadata fully describes the data set and scientists might end up in a wild-goose chase. Instead, it is attractive to receive a visual preview on the archived data along with its metadata. Here, the visual preview can be a reduced-size version of the large data set, used to help in recognizing and organizing them. Ma discusses a similar approach by realizing an in-situ visualization in which snapshot images are generated alongside with data generation (Ma, 2009).

Our goal is to provide visual previews of large data for easier data browsing. These previews are served interactively, with the capability of delivering high quality visualization in consonance with the user requirement.

In this paper we present a framework that produces large data previews for a broad range of client hardware, covering devices from mobile phones up to powerful desktops. Our framework, WAVE [1], provides an adaptive solution that tunes the visual quality according to available client resources, network bandwidths, and user demands. In particular, we balance the processing loads at offline data preprocessing (batch jobs), online server data preparation, and client visualization.

We address interactive scalability for data browsing and data analysis for a broad range of client hardware. Due to the diversity of client hardware requirements, the size of the supporting data also differs accordingly. In response, we use *multi-resolution slicemap*, exchanged between the server and the client, as our main data object (Congote et al., 2011). The *slicemap* is a 3D data structure in the form of a mosaic-format image, which is composed from a series of cross-section images. Rather than generating each *slicemap* intended for the final display, we precompute a whole hierachy of *mutiresolution*

[1]The name WAVE stands for Web-based Analysis of Volumetric Extraction.

Tan Jerome N., Chilingaryan S., Shkarin A., Kopmann A., Zapf M., Lizin A. and Bergmann T.
WAVE: A 3D Online Previewing Framework for Big Data Archives.
DOI: 10.5220/0006228101520163
In *Proceedings of the 12th International Joint Conference on Computer Vision, Imaging and Computer Graphics Theory and Applications (VISIGRAPP 2017)*, pages 152-163
ISBN: 978-989-758-228-8
Copyright © 2017 by SCITEPRESS – Science and Technology Publications, Lda. All rights reserved

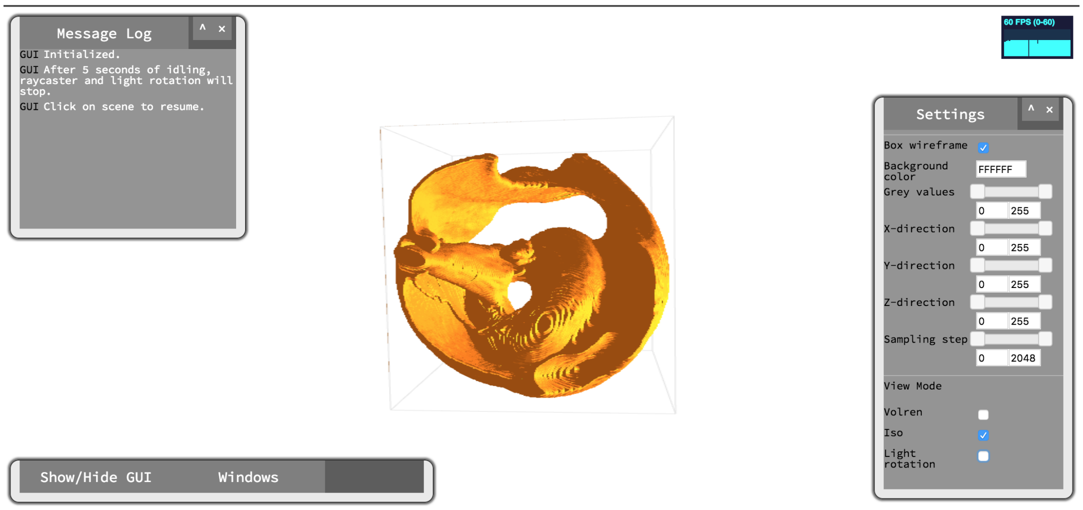

GUI Initialized.
GUI After 5 seconds of idling, raycaster and light rotation will stop.
GUI Click on scene to resume.

Box wireframe	✓
Background color	FFFFFF
Grey values	0 255
X-direction	0 255
Y-direction	0 255
Z-direction	0 255
Sampling step	0 2048
View Mode	
Volren	☐
Iso	✓
Light rotation	☐

Figure 1: A biological screw found in a bettle's leg (van de Kamp et al., 2011) rendered by the WAVE client user interface using the surface rendering method.

slicemaps as caches instead. In order to achieve an optimal visual quality with reasonable performance, our framework selects the cache with a suitable level-of-detail (LOD) by evaluating the visual resolution and the performance of the client graphical device. Moreover, the simplicity of the *slicemap* allows us to optimize processing tasks between the server and the client by minimizing data transfers and server loads for better scalability. The server loads are further alleviated as we prepare the reduced data set in advance using low-priority batch jobs and cache the data either temporarily or permanently according to the configuration of the system.

By utilizing both the client and the server resources, the WAVE framework is able to produce an interactive 3D preview on most client devices without being restricted neither by the data size nor by the data latency. Our framework supports zoom-on-demand approach, which reloads the user selected region using caches with a high level-of-detail. Further in this paper, we evaluate our framework using a data set from the entomology science experiment. Our framework is open source, and it is generally applicable to other science domains where an interactive 3D web-based data previewer is required.

2 RELATED WORK

In this section, we present relevant works in large data processing that helps in visual data browsing. Two viable approaches to realize our goal are *in-situ visualization* and *multi-resolution techniques* (Childs, 2007).

2.1 in situ Visualization

Rivi et. al. described three different approaches in in-situ visualization: they are *tightly coupled*, *loosely coupled*, and *hybrid* approaches. These approaches are still widely used in many High Performance Cluster (HPC) facilities. There is no single universal technique for in-situ visualization as each approach can be beneficial in each different use case (Rivi et al., 2012).

The *tightly coupled* approach does not require data movement, with visualization and computation running on the same nodes or machine. Numerous applications using this approach can be seen in SciRun (Johnson et al., 1999), Hercule (Tu et al., 2006), ADIOS and CoDS (Zhang et al., 2012), and YT package (Turk et al., 2010). However, this approach requires large investments in visualization equipments and knowledge in the simulation code.

The *loosely coupled* approach on the other hand has separate set of resources involving data movement over the network. For example, data processing is done on the server while images are streamed to the client. This approach offers flexibility but at the expense of being restricted by the network bandwidth. Applications using such approach can be seen in Strawman (Larsen et al., 2015), Image-based approach (Ahrens et al., 2014), Catalyst (Lorendeau et al., 2013), PreDatA and ADIOS (Malakar et al., 2010), and EPSN (Esnard et al., 2006).

The *hybrid* approach is the most similar to the WAVE framework, in which data is reduced in a tightly coupled setting and later sent to a concurrent resource for further post processing. This approach inherits advantages from the *tightly coupled* and the *loosely coupled* approaches, and at the same time

SCITEPRESS SCIENCE AND TECHNOLOGY PUBLICATIONS

minimizes their drawbacks, e.g. ParaViewWeb (Rivi et al., 2012), X3DOM (Behr et al., 2009). Here, web browser can be used as the client resource to render the data. Due to the advancement in web technologies that exploits the power of GPU through WebGL (Khronos, 2011), data can be processed in parallel even on a less powerful mobile device. Congote et al. presented an early work on web-based volume visualization using the GPU-based ray marching approach in WebGL (Congote et al., 2011), which proved to be an interesting option. Being inspired by their work, traits of their work can be seen in our framework, especially the usage of the *slicemap* as our main data object.

2.2 Multi-resolution Techniques

Isenberg et. al. presented an analysis regarding recent visualization techniques and categorized multi-resolution techniques, view-dependent visualization, and level of detail under the main category *abstraction, simplication, approximation* (Isenberg et al., 2017). These subsets of techniques complement each other to achieve an efficient rendering at an interactive rates. Although multi-resolution techniques had been presented early back in 1983 by Williams (Williams, 1983), such approach is still valid, as the system bottleneck continues to remain at the network bandwidth.

In this section, we discuss on applications that utilized these techniques. Burigat and Chittaro studied the feasibility of overview-and-demand visualization on mobile devices (Burigat and Chittaro, 2013). In their study, they firstly loaded a map with the coarsest level of detail, and a map with better level of detail only on a higher zoom level.

Lu et. al. introduced a flexible LOD control scheme to effectively explore the flow structures and characteristics on programmable graphics hardware (Lu et al., 2015). In their control scheme, the output textures were created according to a sparse noise model, taking the depth distance of a point and the corresponding brick contribution into consideration.

Kimball et. al. introduced a level of detail algorithm which enables interactive visualization of massive, unstructured, particle data sets (Kimball et al., 2013). They created a multi-resolution pyramid of volume slabs and stacked them into volumes. Each slabs vary in level of detail and full resolution slabs are used at the closest view.

Zinsmaier et. al. proposed a technique that allows straight-line graph drawings to be rendered interactively with adjustable level of detail (Zinsmaier et al., 2012). They used the density-based node aggregation and the edge aggregation to select visual patterns at different levels of detail. They were able to show graphs with up to $\sim$ 107 nodes and up to $\sim$ 106 edges at interactive rates.

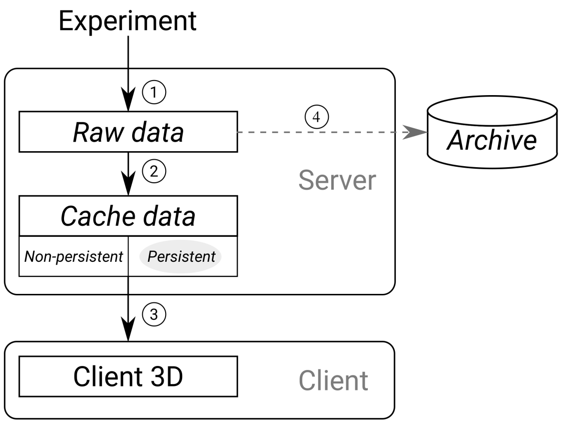

Figure 2: The data flow of the WAVE framework.

All these applications first prepared a series of LOD data governed by its varying visual detail, e.g. resolution. A control logic was then applied to select the best LOD data according to the intended visualization. In the WAVE framework, we also prepare a hierarchy of *multi-resolution slicemaps* varying in its image resolution. A cache selection is put into action to select the best *slicemap* according to the client hardware.

3 THE WAVE FRAMEWORK

An effective large data previewing framework must address two main challenges: they are large data processing and interactive scalability across various client hardware. The large data can be either processed in parallel or reduced in size. We use the latter approach, where our framework mainly processes the data at the offline data preprocessing stage, the online server data preparation stage, and the client visualization stage.

As shown in Figure 2, the offline data preprocessing stage monitors new incoming data from the experiment using a cron service (Step 1) and caches the LOD data (Step 2). Depending on the client performance, our framework selects the best cache data that provides a good visual quality and a reasonable bandwidth transmission (Step 3). The client visualization stage then render the selected data by performing a direct volume rendering or a surface rendering. During the online server data preparation stage, a high-resolution *slicemap* is generated on-the-fly upon user demand. The generated *slicemap* uses the cache data

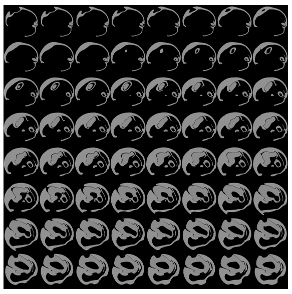
Figure 3: An 8×8 *slicemap* of a biological screw (van de Kamp et al., 2011).

to reduce the wait time.

To deal with the growing data size in the server storage, data that are no longer in active use, are pushed to a dedicated remote archive (Step 4). At the same time, non-persistent caches are flushed while preserving persistent caches. These persistent cache data are later served as a list of visual previews for remote data browsing.

Throughout our framework, the usage of the *slicemap* is motivated by the lack of 3D texture support in the WebGL. This restriction led us to emulate the 3D texture by utilizing the available 2D texture feature. By packing the image slices into mosaic format (*slicemap*), we load these *slicemaps* into the texture memory and and use the pixel shader to calculate the x,y coordinate from the z coordinate of the corresponding *slicemap*. For example, a $256 \times 256 \times 64$ volume constitutes a *slicemap* with 2048×2048 pixels arranged as an 8×8 grid of 256×256 pixels image slice. Figure 3 shows an 8×8 *slicemap* generated from a segmented biological screw data (van de Kamp et al., 2011).

3.1 Server Architecture

Figure 4 shows the WAVE server architecture, where each data set undergoes the data reduction, the data caching, and the data thresholding stages before serving the *slicemap* to the client.

Starting from the raw data stage, a cron service monitors incoming new data sets and triggers a series of batch jobs. These batch jobs are mainly discussed in the data reduction stage (Section 3.1.1), where the data size is reduced and transformed into cache formats. These formats are categorized as *low-resolution slicemap*, *high-resolution slicemap*, and *downscaled volume*. With cache data readily available, our framework performs progressive loading by loading a *low-resolution slicemap* first, followed by a suitable *high-resolution slicemap* loading in the background. The suitable *high-resolution slicemap* in this context refers to the *slicemap* that satisfies the client

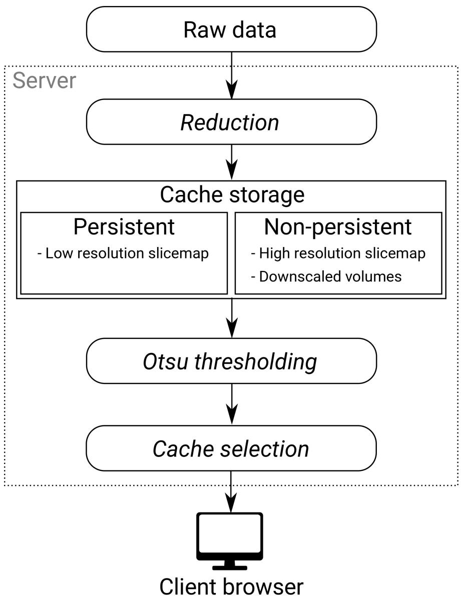

Figure 4: Detailed server architecture.

hardware requirement.

We also allow online generation of *slicemap* with level of detail higher than the *high-resolution slicemap* in the zoom-on-demand approach (Section 3.3). During the online *slicemap* generation, the cached *downscaled volume* is used to minimize the wait time. Only the *low-resolution slicemap* is stored as a persistent cache, whereas the other caches are non-persistent. While each raw data is stored in a folder, we store its respective caches within its folder as well.

3.1.1 Data Reduction

Due to the large data size, we downscaled the raw data before transforming it into a *slicemap*. We used the Lanczos filter from ImageMagick to perform the downscaling operation. After downscaling, we transformed the *downscaled volumes* into a PNG-format *slicemap*. For example, a raw data set of a carpenter ant (Garcia et al., 2013) with $2016 \times 2016 \times 2016$ voxels (7.7 GB) can be downscaled and transformed into a *low-resolution slicemap* with $256 \times 256 \times 256$ voxels (2 MB). Figure 5 shows the processing time of each operation during the online server data preparation performed on a 64 bit Quad-Core Intel(R) Core i7-3770 CPU at 3.40 GHz. These operations are discussed more in Section 3.3. Our initial study shows that the time taken to perform the downscaling operation is much higher than the others, which motivates us to precompute a set of downscaled volumes as caches. In our framework, we had chosen *downscaled volumes* with 256^3 voxels, 512^3 voxels, 768^3

Table 1: Relationship between the varying size of the *slicemap* and the frame rate of the client devices.

Device (GPU)	Texture Unit	Texture Size (pixels)	GFXbench[a] (frames)	Voxels (fps)		
				128^3	256^3	512^3
Desktop (Titan)	32	16384^2	107898	1301	649	245
Laptop (GT750M)	16	16384^2	8821	200	112	45
Desktop (HD4000)	16	8192^2	3362	102	32	11[b]
Phone (Adreno330)	16	4096^2	1601	30	12[b]	1[b]

[a] The frame metrics are taken from GFXBench benchmarking suite tested with *T-Rex off-screen 1080p* (Kishonti, 2011). This metric shows the performance of each GPU (higher the better).

[b] <15fps. Unacceptable user perception quality (Claypool et al., 2006).

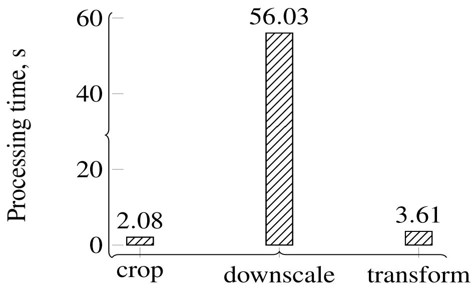

Figure 5: Online server data preparation of a $2016 \times 2016 \times 2016$ voxels carpenter ant data set (Garcia et al., 2013).

voxels, and 1024^3 voxels. By having *slicemaps* and *downscaled volumes* as caches, our framework is able to serve data at an interactive rate.

3.1.2 Multi-resolution Support

To support a broad range of clients with varying hardware, *multi-resolution slicemaps* that vary in resolution details are created. As the size for *slicemaps* may differ according to the client hardware, we performed a study on the relationship between the varying size of *slicemaps* and the frames-per-second of various client devices. Here, we had chosen a broad range of client devices, covering from less powerful mobile phone up to powerful desktop. The performance of each client device rendering multiple data sizes is shown in Table 1. In this study, we assumed that the data size is inversely proportional to the scale of data transmission. In other words, a small data size results in a high data transmission, whereas a larger data size results in a lower data transmission. Detailed time taken in data transmission for various *slicemap* sizes under different network presets is shown later in Section 4. We determine the user acceptance metric base on the study conducted by Claypool et al.. In their study, the user performance and the user perception quality dropped significantly when the frames-per-second is below 15fps (Claypool et al., 2006).

As shown in Table 1, the data set with 128^3 voxels provides the best frames-per-second across the selected client devices; data sets with 256^3 voxels and 512^3 voxels are imposing problems on the smaller client device. However, data set with 128^3 voxels delivered a visual object that is no longer recognizable leading us to select a *slicemap* with 256^3 voxels as the low-resolution slicemap, and higher voxel size as *high-resolution slicemaps*. Although the data set with 256^3 voxels had an unacceptable frames-per-second (<15fps) on the mobile device, but we can further improve the client rendering with an optimized code. Though it may seem that only two data sizes are available as cache levels, we vary the z-axis to give us more granularity for gradual visual improvement. We define a hierarchy of levels varying in the amount of voxels. With N levels of slicemaps, each *level N slicemap* contains $256^3 \times 2^N$ voxels. In our framework, we precompute four levels of *slicemaps* to cover most client resources (Table 2). Our scheme can be further extended depending solely on the advancement of the hardware.

Table 2: Multi-resolution hierarchy scheme definition.

Level	Scheme	Voxels	Format
0	$256^3 \times 2^0$	16777216	$256 \times 256 \times 256$
1	$256^3 \times 2^1$	33554432	$256 \times 256 \times 512$
2	$256^3 \times 2^2$	67108864	$512 \times 512 \times 256$
3	$256^3 \times 2^3$	134217728	$512 \times 512 \times 512$

In the cache selection stage, a suitable *slicemap* is selected depending on the client hardware requirement. There are two parameters that determine the client performance: texture size and texture unit. The texture size defines the image resolution of the *slicemap*, whereas the texture unit defines the amount of *slicemaps* that can be rendered. To select the suitable *slicemap* level, the product of the texture unit and the texture size of the mobile device is used as our *baseParameter* ($16 \times 4096 = 65536$). We then compute the appropriate cache level by $\lfloor \log_2 \frac{clientTextureUnit \times clientTextureSize}{baseParameter} \rfloor$, where $clientTextureUnit$ and $clientTextureSize$ are acquired from the client hardware requirements.

3.1.3 Data Thresholding

We are mostly dealing with electron microscopy images of biological specimens, that are especially noisy

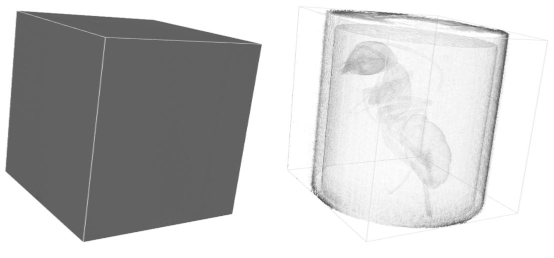
(a) Grey value: 0 - 255 (b) Grey value: 107 - 255

Figure 6: A 3D volume rendering without (a) and with (b) Otsu thresholdings. The calculated Otsu threshold is 107.

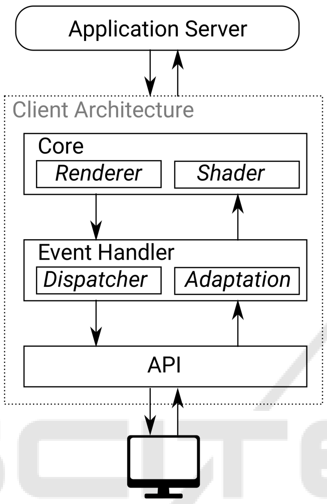

Figure 7: Detailed client architecture.

and low contrasted (Coudray et al., 2010). With no prior knowledge of the region of interest, our visual previewer framework might end up showing all available grey values from the data set, rendering a 3D object that fills up the entire volume as shown in Figure 6a. Under such circumstances, the user can filter out the grey values using the WAVE interface settings (Figure 1). However, a visual previewer framework that requires manual thresholding from users is not easy to use. Instead, we adopt the Otsu thresholding method on our *low-resolution slicemap*.

The Otsu thresholding method tries to minimize the combine spread between the two clusters by moving the threshold along the grey value range (within-class variance). We chose another variation of the Otsu method that depends only on the difference between the means of the two clusters, thus avoiding the need to calculate differences between individual intensities and the cluster means (Morse, 2000). This variant is described in (1).

$$\sigma^2_{Between}(T) = n_B(T)n_O(T)[\mu_B(T) - \mu_O(T)]^2 \quad (1)$$

where T is the varying threshold along the range of grey values. $\sigma^2_{Between}$ is the mean difference between the two clusters. $n_B(T)$ is the sum of pixels in the background (below threshold). $n_O(T)$ is the sum of pixels in the foreground (above threshold). $\mu_B(T)$ and $\mu_O(T)$ are variances of pixels in background (below threshold) and foreground (above threshold), respectively. We select the threshold that gives us the highest mean difference between the two clusters.

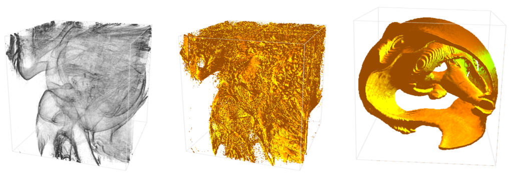
(a) (b) (c)

Figure 8: A 3D visualization of segmented and non-segmented biological screw data sets using the volume rendering and the surface rendering methods. (a) Volume rendering with raw data set. (b) Surface rendering with raw data set. (c) Surface rendering with segmented data set.

Although one might argue that the Otsu thresholding method should be performed on the raw data. But, we achieved great success performing the Otsu method on the *low-resolution slicemap*, in which the correct threshold value is acquired in a much shorter time. This threshold value can be applied to all other *slicemaps* stemming from the same raw data. Figure 6b shows a 3D object rendered with an Otsu threshold of 107. It is worth noting that the threshold value serves as a reference for the minimum grey value, and user still has the option to change the threshold value through the WAVE user interface.

3.2 Client Architecture

Our WAVE client is implemented in Javascript, which is written on top of the ThreeJS library (Cabello, 2011) that utilizes WebGL (Khronos, 2011). The Javascript language offers platform independence, and it can be interpreted at every major client browser. Figure 7 depicts our client architecture, which is consist of a core layer, an event handler layer, and an application programming interface (API) layer. The core layer is responsible for rendering the *slicemap*. Within the core layer, the renderer and the shader components perform the direct volume rendering based on the work from Kruger and Westermann (Kruger and Westermann, 2003) and the local surface illumination model using the Blinn-Phong model (Blinn, 1977). Figure 8 shows 3D visualizations of both raw and segmented biological screw data sets in both volume rendering and surface rendering modes. Although we support both the volume rendering and the surface rendering methods, the volume rendering method is more suited to visualize new data set due to its ability to inspect the inner structure; The surface rendering method provides an attractive visual

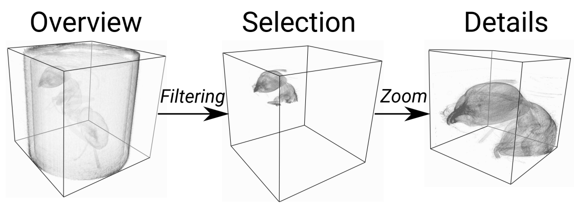

Figure 9: An illustration of zoom-on-demand feature.

quality on the segmented data set (Figure 8c).

In the volume rendering approach, ray is emulated and sampled with a constant step size. These sampled points then contribute to the final composition function. By varying the step size, the performance and visual detail of the rendered object can be adapted accordingly. This is a matter of trade off between performance and visual detail, where large step size leads to faster rendering but less visual details. We reduce the step size during a dynamic 3D object movement and increase the step size when the object is static.

In order to facilitate user interactions from the browser, the WAVE client provides a set of API. These API calls allow the user to configure the core layer from the browser directly. Furthermore, they provide an easy integration into a variety of web applications with varying designs and layouts, e.g. Biomedisa web application (Lösel and Heuveline, 2016). In the event handler layer, the adaptation component and the dispatcher component handle the user state and the core layer state between the WAVE client and the user interface. In particular, our client framework provides four features to inspect and analyze the data set: (a) by selecting the grey value threshold, (b) by adjusting the transfer function, (c) by changing the camera position and (d) by slicing through the 3D object. The first feature (a) is useful to inspect a new data set, where the grey value threshold is selected to remove the unwanted background. The second feature (b) enables transfer function update (Pfister et al., 2001); Each grey value is assigned a colour according to the selected function to help in classification of the data set. The third feature (c) changes the camera position of the viewer in the 3D scene allowing the user to view the 3D data in any angle and distance. The last feature (d) slices through the 3D object in x, y and z-directions providing flexibility for the user to inspect the inner structure of the data set.

3.3 Zoom on Demand

The WAVE framework supports the zoom-on-demand approach, which follows the visual information seeking mantra, *overview first, zoom and filter, then details-on-demand* (Shneiderman, 1996). The zoom-on-demand approach allows the user to select a region of interest from the 3D volume for more details (Figure 9). Using the browser cache (*high-resolution slicemap*), a new *slicemap* is initally generated consisting of the selected region, where the number of slices is determined and each image slice is cropped accordingly. These operations are performed locally in the client browser using the JavaScript language. At the same time, another *slicemap* with higher details containing the selected region is created from the server (online server data preparation). The online server data preparation uses the readily cached *downscaled volume* for fast *slicemap* generation.

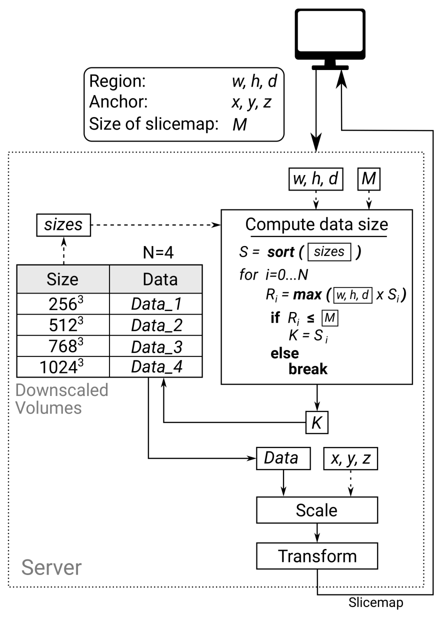

Figure 10: Selection of the cached *downscaled volumes* according to client requirements.

To select the *downscaled volume*, the intended *slicemap* size, M, the selected region parameters, $[w,h,d]$, and the anchor points, $[x,y,z]$, are acquired from the client, where x, y, z are the starting points of the selected region; and w, h, d are the width, height and depth of the selected region $(x,y,z,w,h,d \in [0,1])$. Figure 10 shows the process to select the suitable *downscaled volume*. To compute the suitable *downscaled volume* size, we iterate through all the sizes from 256 to 1024. At each iteration, we select the product of the region parameters, $[w,h,d]$, and the current iterated size, S_i, that is less than the size of the intended *slicemap*, M. Whenever the current iterated size, S_i, is larger than the intended size, M, the previous iterated size is selected. The selected *downscaled volume* is then scaled according to the region parameters and the anchor points. Lastly, the scaled data is transformed into the intended *slicemap* format before serving it back to the client.

SCIENCE AND TECHNOLOGY PUBLICATIONS

Table 3: A series of *slicemaps* produced from the carpenter ant data set (Garcia et al., 2013) in the WAVE server.

Category	Scheme	Voxels	Slicemap Size	Reduction Ratio[a]
Low-resolution (*level 0*)	$256 \times 256 \times 256$	16777216	1.90 MB	488
High-resolution (*level 1*)	$256 \times 256 \times 512$	33554432	3.90 MB	244
High-resolution (*level 2*)	$512 \times 512 \times 256$	67108864	9.70 MB	122
High-resolution (*level 3*)	$512 \times 512 \times 512$	134217728	20.10 MB	61

[a] Reduction ratio is used to quantify the reduction in data representation size (voxels) produced from the WAVE server. The raw data set consisted of $2016 \times 2016 \times 2016$ voxels. $ReductionRatio = \frac{rawAmountVoxels}{reducedAmountVoxels}$

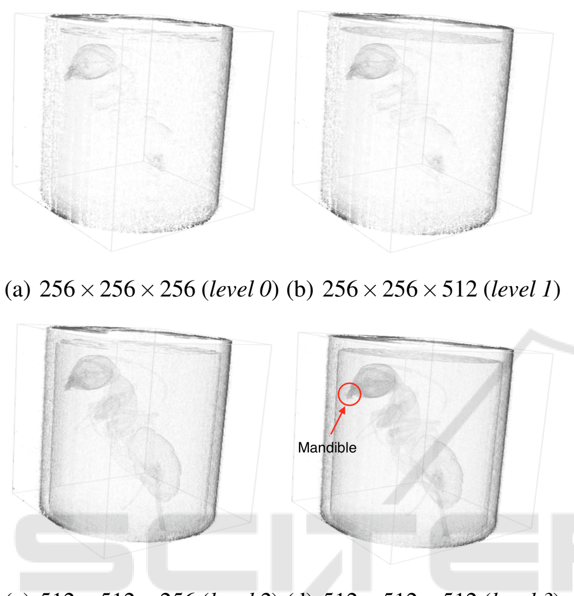

(a) $256 \times 256 \times 256$ (*level 0*) (b) $256 \times 256 \times 512$ (*level 1*)

(c) $512 \times 512 \times 256$ (*level 2*) (d) $512 \times 512 \times 512$ (*level 3*)

Figure 11: Four 3D objects of a carpenter ant (Garcia et al., 2013) rendered from our *multi-resolution slicemaps*: (a) AE: 0, RMSE: 0%, base image, (b) AE: 90264, RMSE: 0.049%, (c) AE: 178678, RMSE: 0.060%, and (d) AE: 201959, RMSE: 0.068%.

4 EVALUATION

The WAVE framework is currently implemented in the Astor web portal (Astor, 2014), in the USCT application (Ruiter et al., 2013) and also in the Biomedisa online segmentation application (Lösel and Heuveline, 2016). To illustrate the image quality and the performance delivered by our framework, we selected a carpenter ant data set (Garcia et al., 2013) with 2016^3 voxels. The carpenter ant belongs to the order of *Hymenoptera* under the family of *Formicidae*. This raw data was transformed into a series of *slicemaps* according to our multi-resolution scheme definition (Table 3). A set of *downscaled volumes* were also cached in the server. Throughout our evaluation, we used a 64 bit Quad-Core Intel(R) Core i7-3770 CPU at 3.40 GHz as our server, and a MacbookPro running on a NVIDIA GeForce GT750M as our client.

4.1 Visual Quality

Serving as a large data previewing framework, our framework must be able to present a recognizable visual object using our hierarchy of *multi-resolution slicemaps*. Also, the zoom-on-demand approach must provide more details on the selected sub-region.

The visual quality of the WAVE framework is determined according to the amount of pixels rendered on the browser screen. More pixels imply that more details are rendered, thus giving us a better preview. We used the absolute error count metric (AE) to show the number of different pixels in a masked image. The mask image refers to a resultant image from masking the test image against a base image. Also, we used the root mean squared error (RMSE) to show the gradual visual improvement in our framework approaches. We performed these widely used image quality metrics on 3D object screenshots rendered by *multi-resolution slicemaps* and zoom-on-demand *slicemaps*.

Figure 11 shows previews of the carpenter ant rendered by our *multi-resolution slicemaps*, from level 0 to level 3. Here, the *low-resolution slicemap*, *level 0*, was selected as the base image tested against four *multi-resolution slicemaps*. Although the *low-resolution slicemap* (level 0) has lesser details, the structure still resembles the carpenter ant. The mandible of the carpenter ant is visible in all rendered objects. Nevertheless, we can see a gradual visual improvement from *level 0* to *level 3*. The gradual visual improvement is also indicated from the increasing value of AE and RMSE.

We further evaluated the zoom-on-demand approach, in which 3D object with higher details are created from browser cached *slicemap* and later from server cached *downscaled volume*. Figure 12 shows the upper body of the carpenter ant rendered from browser cached *multi-resolution slicemaps* from *level 0* to *level 3*. Although the *level 2 slicemap* object had a higher AE and RMSE values than the *level 3 slicemap* object, the smooth edges in the *level 3 slicemap* object lent itself to a lesser masked region,

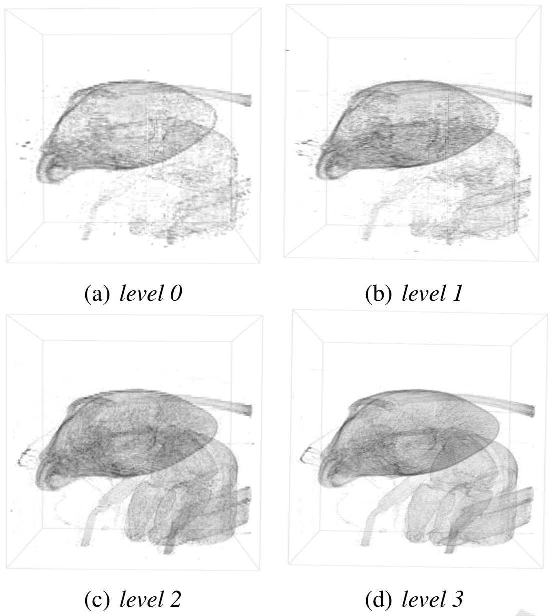

Figure 12: The visual quality of the zoomed carpenter ant (upper body) created by *multi-resolution slicemaps* in the client browser using the JavaScript language: (a) AE: 0, RMSE: 0%, base image, (b) AE: 126586, RMSE: 0.055%, (c) AE: 160369, RMSE: 0.080%, and (d) AE: 159571, RMSE: 0.069%.

thus resulting in a slightly smaller AE and RMSE values.

During the zoom-on-demand, our framework triggered a request to the server for a *slicemap* with better quality. In this particular test, our client was running on a GTX Titan graphic card with a *texture unit* and *texture size* of 32 and 16384px, respectively. Thus, the cache level suitable for our client is $\lfloor \log_2 \frac{32 \times 16384}{65536} \rfloor = 3$. The *level 3 slicemap* consists of $512 \times 512 \times 512$ voxels, resulting in M value of 134217728. We selected the zoom region (carpenter ant's head) using the WAVE user interface and sent $[x, y, z, w, h, d] = [0.15, 0.43, 0.62, 0.38, 0.38, 0.38]$ to the server. Base on the selection algorithm shown in Figure 10, the *downscaled volume* of size 1024^3 was selected. Figure 13 compares the visual quality of 3D objects rendered from the browser cached and the server cached *slicemaps* using the same set of parameters.

The results showed that the WAVE framework is capable of delivering recognizable visual previews from the large data using the prepared *multi-resolution slicemaps*. Even the 3D objects rendered by the newly generated *slicemaps* from the browser cached *slicemap* and the server cached *downscaled volume* are able to provide more visual details for further analysis.

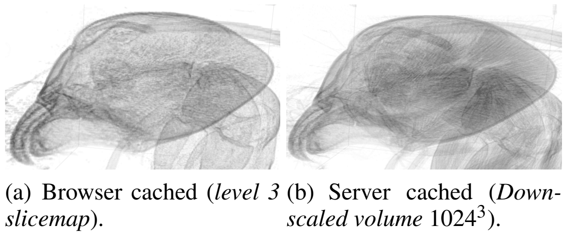
(a) Browser cached (*level 3 slicemap*).
(b) Server cached (*Downscaled volume* 1024^3).

Figure 13: A comparison between a browser cached (*level 3 slicemap*) and a server cached (*Downscaled volume* 1024^3) on a client (GTX Titan) with $M = 512 \times 512 \times 512$ and $[x, y, z, w, h, d] = [0.15, 0.43, 0.62, 0.38, 0.38, 0.38]$. The selected region is the carpenter ant's head. (a) RMSE: 0.24%, (b) RMSE: 0.29%. A white image is used as the base image to perform image quality comparison.

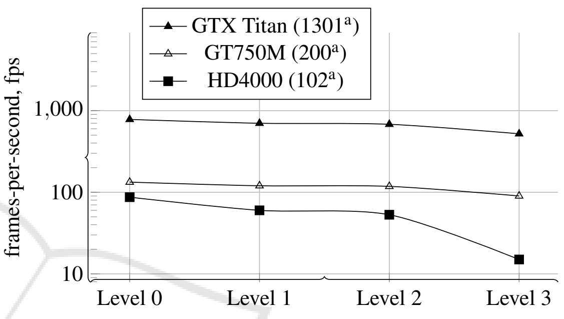

Figure 14: The frames-per-second for *multi-resolution slicemaps* on various client resources (sampling step=256). [a] refers to the frame metrics from the WAVE framework tested against each client hardware with a test data size of 128^3 voxels (the higher the better).

4.2 Performance

The WAVE performance is determined mainly by the user experience, which is related to the system interactivity and latency. The first tests measure the responsiveness of the client-side rendering; this represents average frame rates across various client devices. However, frame rate alone does not give us an overview of the overall performance. The latency between server-client interaction also affects the perceived system interactivity. Hence, we performed tests to measure the page load time for various data sizes, and to measure the total time taken to perform the online server data preparation (zoom-on-demand).

4.2.1 Frame Rates

The rendering performance of the client hardware is related to the *slicemap* size, the volume rendering sampling step size, and the GPU hardware.

Figure 14 shows the frame rate of our *multi-resolution slicemaps* rendered on various client hardware. From the result shown, the *slicemap* containing

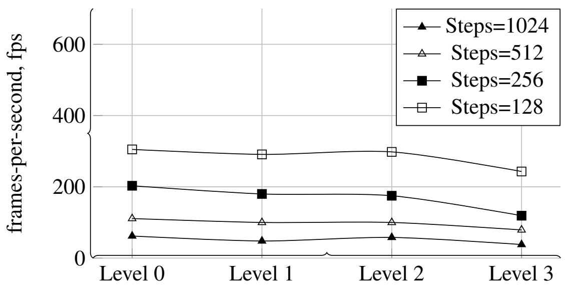

Figure 15: The frames-per-second for various *slicemaps* by varying sampling steps in MacbookPro (GT750M).

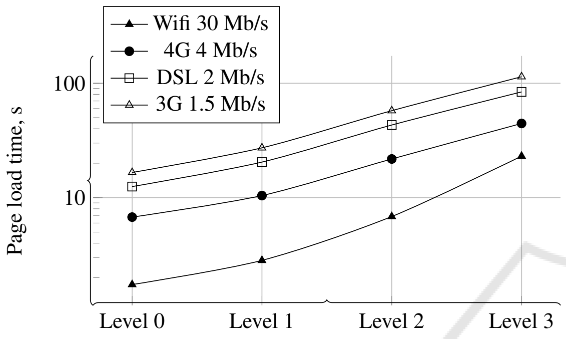

Figure 16: Latency for *multi-resolution slicemaps* on different network presets.

higher details requires better client hardware for better performance. We also showed the relationship between varying sampling step size and the frame rate on a MacbookPro running on a NVIDIA GeForce GT750M (Figure 15). This test is only valid for the volume rendering mode, as the surface rendering mode stops at the first ray intersection point.

4.2.2 Latency

Figure 16 shows the data latency between the server and the client serving *multi-resolution slicemaps* under different network presets. Although our framework offers a hierarchy of *slicemaps* to ensure interactive response across a broad range of clients, the higher *slicemap* levels require a good network connection to be effective.

According to the client hardware, a *high-resolution slicemap* selected by $\lfloor \log_2 \frac{clientTextureUnit \times clientTextureSize}{baseParameter} \rfloor$ is loaded. By zooming onto the upper body of the carpenter ant ($[x,y,z,w,h,d] = [0.15, 0.43, 0.62, 0.38, 0.38, 0.38]$), our framework first creates a new *slicemap* from the browser cached *high-resolution slicemap*. Figure 17 shows each *slicemap* generation time from its browser cached *high-resolution slicemap*. Then, our client requested for a *slicemap* with higher details from the server. In practice, our framework selects the best *downscaled volume* based on the selection algorithm in Figure 10. However, we showed the processing latency of the online server data preparation from the raw data and all available *downscaled volumes*: 256^3, 512^3, 768^3, and 1024^3 (Figure 18). The result showed an improvement of approximately 50 seconds by using the *downscaled volume* cache in contrary to creating the *slicemap* directly from the raw data. However, there is not much difference ($\sim$ 3 seconds) in performance between using the *downscaled volume* of 256^3 or the *downscaled volume* of 512^3.

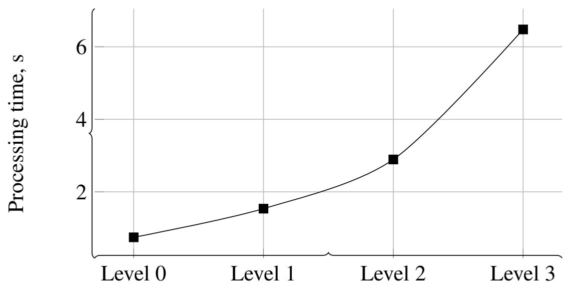

Figure 17: Performing zoom-on-demand on the client-side (Javascript) using the browser cached *high-resolution slicemap*.

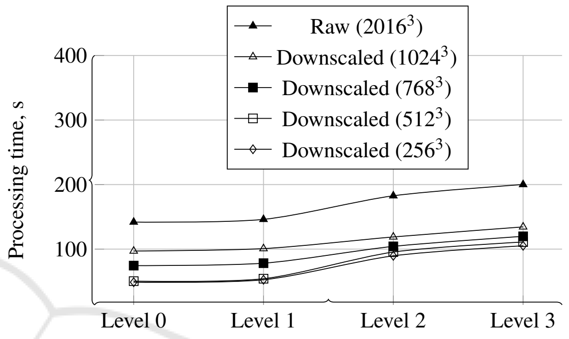

Figure 18: The data latency in performing the online server data preparation from server cached *downscaled volumes*.

The results so far showed the importance of first loading the *low-resolution slicemap* (*level 0*) that has a much lower latency across various network presets and renders much faster on various client hardware. We also showed the benefit of using the browser cached *slicemap* to create the new zoomed *slicemap*, while a better *slicemap* was being created using the *downscaled volume* (server cache).

5 CONCLUSIONS AND FUTURE WORK

We have presented a 3D visual previewing framework for big data archives that promotes data availability across various clients. The WAVE framework supports the volume rendering and surface rendering, which are useful in identifying a new data or a postprocessed data. Moreover, our framework allows zoom-on-demand where user can reload a selected region with higher visual details. To support the diverse client hardware, we introduced a hierarchy of *multi-resolution slicemaps* mainly for the progressive loading approach, in which the *low-resolution slicemap* is displayed first while a suitable *high-resolution slicemap* is loading in the background. By performing the offline data preprocessing at the server side, the framework can provide previews on large data set at an interactive rate. The offline data preprocessing is responsible in reducing the large data size and prepares a series of cache data. These cache data are essential to perform the progressive loading and the online server data preparation (zoom-on-demand). The visual results and performances of the WAVE framework were promising, which strongly suggested the WAVE framework being an effective visual previewer framework.

In future work, we plan to support interactive labeling and commenting directly on the biology object via our user interface, steering our framework into becoming a distributed synchronous collaboration tool (Isenberg et al., 2011). We also would like to introduce new rendering schemes that open up more visualization opportunities for better data inspection and analysis. One of the highlights in our work is the usage of *slicemap* as our main data object. We could simplify the in-situ visualization approach by producing multiple intermediate *slicemaps* to monitor the progress of a simulation or segmentation process. As our *slicemap* is in an image format, we would further improve the image compression technique for better data latency over the network, e.g. compressing image slices into a video. Although the Otsu thresholding method performed seemingly well in our framework, extending the spectrum of thresholding methods is by all means beneficial (Rosin, 2001; Coudray et al., 2010). Furthermore, an automated heuristic is an attractive addition to the WAVE framework, which selects a rendering method and settings based on the server performance, the network bandwidth, the client hardware and the user needs.

ACKNOWLEDGMENTS

The authors would like to acknowledge Felix Schultze, Alexey Tukalo, Guven Gokdemir and Wu Chengzhi for their contributions to the WAVE framework. We also thank Michael Heethoff, Sebastian Schmelzle, Thomas van de Kamp, Nicole Ruiter and Torsten Hopp for helpful discussions on their experiment data sets.

REFERENCES

Ahrens, J., Jourdain, S., O'Leary, P., Patchett, J., Rogers, D. H., and Petersen, M. (2014). An image-based approach to extreme scale in situ visualization and analysis. In *Proceedings of the International Conference for High Performance Computing, Networking, Storage and Analysis*, pages 424–434. IEEE Press.

Astor (2014). Astor web portal. https://anka-astor-portal.anka.kit.edu/.

Behr, J., Eschler, P., Jung, Y., and Zöllner, M. (2009). X3dom: a dom-based html5/x3d integration model. In *Proceedings of the 14th International Conference on 3D Web Technology*, pages 127–135. ACM.

Blinn, J. F. (1977). Models of light reflection for computer synthesized pictures. In *ACM SIGGRAPH Computer Graphics*, volume 11, pages 192–198. ACM.

Burigat, S. and Chittaro, L. (2013). On the effectiveness of overview+ detail visualization on mobile devices. *Personal and ubiquitous computing*, 17(2):371–385.

Cabello, R. (2011). Threejs. https://threejs.org/.

Childs, H. (2007). Architectural challenges and solutions for petascale postprocessing. In *Journal of Physics: Conference Series*, volume 78, page 012012. IOP Publishing.

Claypool, M., Claypool, K., and Damaa, F. (2006). The effects of frame rate and resolution on users playing first person shooter games. In *Electronic Imaging 2006*, pages 607101–607101. International Society for Optics and Photonics.

Congote, J., Segura, A., Kabongo, L., Moreno, A., Posada, J., and Ruiz, O. (2011). Interactive visualization of volumetric data with webgl in real-time. In *Proceedings of the 16th International Conference on 3D Web Technology*, pages 137–146. ACM.

Coudray, N., Buessler, J.-L., and Urban, J.-P. (2010). A robust thresholding algorithm for unimodal image histograms. *Pattern Recognition Letters*, (31):1010–1019.

Esnard, A., Richart, N., and Coulaud, O. (2006). A steering environment for online parallel visualization of legacy parallel simulations. In *2006 Tenth IEEE International Symposium on Distributed Simulation and Real-Time Applications*, pages 7–14. IEEE.

Garcia, F. H., Wiesel, E., and Fischer, G. (2013). The ants of kenya (hymenoptera: Formicidae)-faunal overview, first species checklist, bibliography, accounts for all genera, and discussion on taxonomy and zoogeography. *Journal of East African Natural History*, 101(2):127–222.

Isenberg, P., Elmqvist, N., Scholtz, J., Cernea, D., Ma, K.-L., and Hagen, H. (2011). Collaborative visualization: definition, challenges, and research agenda. *Information Visualization*, 10(4):310–326.

Isenberg, P., Isenberg, T., Sedlmair, M., Chen, J., and Möller, T. (2017). Visualization as seen through its research paper keywords. *IEEE Transactions on Visualization and Computer Graphics*, 23(1).

Johnson, C., Parker, S. G., Hansen, C., Kindlmann, G. L., and Livnat, Y. (1999). Interactive simulation and visualization. *Computer*, 32(12):59–65.

Khronos (2011). WebGL - OpenGL ES 2.0 for the Web, https://www.khronos.org/webgl/.

Kimball, J., Duchaineau, M., and Kuester, F. (2013). Interactive visualization of large scale atomistic and cosmological particle simulations. In *Aerospace Conference, 2013 IEEE*, pages 1–9. IEEE.

Kishonti (2011). Gfxbench 4.0. https://gfxbench.com/.

Kruger, J. and Westermann, R. (2003). Acceleration techniques for gpu-based volume rendering. In *Proceedings of the 14th IEEE Visualization 2003 (VIS'03)*, page 38. IEEE Computer Society.

Larsen, M., Brugger, E., Childs, H., Eliot, J., Griffin, K., and Harrison, C. (2015). Strawman: A batch in situ visualization and analysis infrastructure for multi-physics simulation codes. In *Proceedings of the First Workshop on In Situ Infrastructures for Enabling Extreme-Scale Analysis and Visualization*, pages 30–35. ACM.

Lorendeau, B., Fournier, Y., and Ribes, A. (2013). In-situ visualization in fluid mechanics using catalyst: A case study for code saturne. In *LDAV*, pages 53–57.

Lösel, P. and Heuveline, V. (2016). Enhancing a diffusion algorithm for 4d image segmentation using local information. In *SPIE Medical Imaging*, pages 97842L–97842L. International Society for Optics and Photonics.

Lu, D., Zhu, D., Wang, Z., and Gao, J. (2015). Efficient level of detail for texture-based flow visualization. *Computer Animation and Virtual Worlds*.

Ma, K. L. (2009). In situ visualization at extreme scale: Challenges and opportunities. *IEEE Computer Graphics and Applications*, 29(6):14–19.

Malakar, P., Natarajan, V., and Vadhiyar, S. S. (2010). An adaptive framework for simulation and online remote visualization of critical climate applications in resource-constrained environments. In *Proceedings of the 2010 ACM/IEEE International Conference for High Performance Computing, Networking, Storage and Analysis*, pages 1–11. IEEE Computer Society.

Morse, B. S. (2000). Lecture 4: Thresholding. *Brigham Young University*.

Pfister, H., Lorensen, B., Bajaj, C., Kindlmann, G., Schroeder, W., Avila, L. S., Raghu, K., Machiraju, R., and Lee, J. (2001). The transfer function bake-off. *IEEE Computer Graphics and Applications*, 21(3):16–22.

Ressmann, D., Mexner, W., Vondrous, A., Kopmann, A., and Mauch, V. (2014). Data management at the synchrotron radiation facility anka. In *10th International Workshop on Personal Computers and Particle Accelerator Controls*, PCaPAC 2014.

Rivi, M., Calori, L., Muscianisi, G., and Slavnic, V. (2012). In-situ visualization: State-of-the-art and some use cases. *PRACE White Paper; PRACE: Brussels, Belgium*.

Rosin, P. L. (2001). Unimodal thresholding. *Pattern recognition*, 34(11):2083–2096.

Ruiter, N., Zapf, M., Dapp, R., Hopp, T., Kaiser, W., and Gemmeke, H. (2013). First results of a clinical study with 3d ultrasound computer tomography. In *2013 IEEE International Ultrasonics Symposium (IUS)*, pages 651–654. IEEE.

Shneiderman, B. (1996). The eyes have it: A task by data type taxonomy for information visualizations. In *Visual Languages, 1996. Proceedings., IEEE Symposium on*, pages 336–343. IEEE.

Szalay, A. and Gray, J. (2006). 2020 computing: Science in an exponential world. *Nature*, 440(7083):413–414.

Tu, T., Yu, H., Ramirez-Guzman, L., Bielak, J., Ghattas, O., Ma, K.-L., and O'hallaron, D. R. (2006). From mesh generation to scientific visualization: An end-to-end approach to parallel supercomputing. In *Proceedings of the 2006 ACM/IEEE conference on Supercomputing*, page 91. ACM.

Turk, M. J., Smith, B. D., Oishi, J. S., Skory, S., Skillman, S. W., Abel, T., and Norman, M. L. (2010). yt: A multi-code analysis toolkit for astrophysical simulation data. *The Astrophysical Journal Supplement Series*, 192(1):9.

van de Kamp, T., Vagovič, P., Baumbach, T., and Riedel, A. (2011). A biological screw in a beetle's leg. *Science*, 333(6038):52–52.

Williams, L. (1983). Pyramidal parametrics. In *ACM Siggraph Computer Graphics*, volume 17, pages 1–11. ACM.

Zhang, F., Lasluisa, S., Jin, T., Rodero, I., Bui, H., and Parashar, M. (2012). In-situ feature-based objects tracking for large-scale scientific simulations. In *High Performance Computing, Networking, Storage and Analysis (SCC), 2012 SC Companion:*, pages 736–740. IEEE.

Zinsmaier, M., Brandes, U., Deussen, O., and Strobelt, H. (2012). Interactive level-of-detail rendering of large graphs. *IEEE Transactions on Visualization and Computer Graphics*, 18(12):2486–2495.